PAPER

Check for updates

Gamma-ray dose threshold for MAPbI₃ solar cells†

A. G. Boldyreva, [ID] *[a] A. V. Novikov, [ID] [a] V. G. Petrov, [ID] [b] A. N. Zhivchikova,[a] M. M. Tepliakova [ID] [a] and K. J. Stevenson[b]

In this work, we report on the effects observed in MAPbI₃ polycrystalline films and solar cells under moderate gamma-ray doses of 3–21 kGy. We applied several instrumental techniques such as photoluminescence spectroscopy, time-resolved photoluminescence, Suns-V_{OC} measurement, and impedance spectroscopy to characterize exposed samples. We observed a nonlinear dependency of such characteristics as PL intensity, career lifetime, ideality factor, and recombination resistance on the exposure dose. Small doses of 3–5 kGy annihilate some of the defect centers in the material, which results in improved carrier extraction and prolonged carrier lifetime, while with larger doses of 10 kGy and above, nonradiative recombination becomes predominant. In this way, we revealed a gamma-ray threshold for MAPbI₃ films of around 10 kGy, above which it is not recommended to exploit this material. In space environment, yearly doses rarely exhibit 0.1 kGy (10 krad), and the MAPbI₃ material has a sufficient margin of safety for space applications. Moreover, this unusual behaviour opens up the opportunity to use gamma-ray sources as an effective method to improve the quality of defective polycrystalline perovskite films before actual exploitation in an ionizing radiation-free environment.

Introduction

Complex lead halides with a perovskite structure have been thoroughly investigated in the last 11 years, with particular focus on their application in optoelectronics. Perovskite solar cells continue their race against the world record holder Si-wafer solar cells, which reached 26.8%.[1] In particular, high expectations for perovskite technology are connected with multijunction tandem solar cells as complex lead halides can be adjusted to any desired bandgap from 1 eV for the bottom cell to 3 eV for the top cell. Light weight and low cost make perovskite materials suitable for tandem solar cells not only for terrestrial applications but also for the space industry. It was shown in some early works that perovskite materials such as CH₃NH₃PbI₃·(MAPbI₃) and CH₂N₂H₅PbI₃·(FAPbI₃) are superior to silicon in terms of radiation hardness.[2–4] Some reports claim that perovskite solar cells are stable under high-energy particles due to their impressive defect tolerance and high ionic mobility.[5] Initially defective polycrystalline perovskite films undergo defect annealing (reordering), which results in the healing of some original interstitials and vacancies.[6] In this

regard, studies dedicated to the radiation hardness of perovskite single crystals with less defects are also popular.[7–10]

The space environment depending on the equatorial orbit consists of various ionizing particles that can severely damage solar cell performance. In the lower equatorial orbit LEO, total ionizing dose (TID) is estimated to be around 3–10 krad per year.[11] To imitate space radiation on the Earth, various facilities with different particles and energies are used: protons,[12,13] electrons,[2,14] X-rays[10,15,16] and gamma-rays.[5,7–9,17–22] Normally, electron irradiation is used due to the vast availability of electron beam setups. However, Ahmad R. Kirmani suggested that proton irradiation with low energies up to 1 MeV is a more accurate way to estimate the radiation hardness of perovskites.[23] Indeed, protons (mostly hydrogen ions) are the most common types of particles in space with energies of 0.1–10 MeV and annual fluence of 10^9–10^{10} cm⁻².[23] However, TID testing protocols employed at the European Space Agency use ^{60}Co facilities (gamma source) as the *de facto* standard testing method for all electronics to be used in space.[6] The main reason why Co source was chosen as the etalon for TID testing is due to the highest fraction of unrecombined holes, formed during irradiation. In other words, the most effective method to examine radiation hardness is by exposing samples to a gamma-ray source. Moreover, all other types of particles can be stopped by a glass shield and have minor impact on the material's stability.

Ideally, radiation hardness should be studied *in situ*, as some effects arising from exposure disappear with time.

[a] *Skolkovo Institute of Science and Technology, Nobel Street 3, Moscow 143026, Russia. E-mail: a.boldyreva@skoltech.ru*

[b] *Lomonosov Moscow State University, Department of Chemistry, Leninskie Gory 1 bld. 3, Moscow 119991, Russia*

† Electronic supplementary information (ESI) available. See DOI: https://doi.org/10.1039/d4cp00524d

However, in the case of the gamma-ray source *in situ* measurements are difficult due to the specific design of ionization cells (shielded small chambers). According to the standard TID testing protocol, the measurements should be performed twice: within 1–2 hours after the exposure and after annealing at room temperature.[6]

In our previous study, we compared the stability of several perovskite structures under gamma-ray doses up to 1 Mrad or 10 kGy. We found that MAPbI$_3$-based solar cells are stable under such doses and do not exhibit any degradation except substrate darkening.[5] Herein, we continue studying the radiation hardness of MAPbI$_3$ material in more detail, with a focus on recombination dynamics, employing such advanced methods as time-resolved photoluminescence spectroscopy (TRPL), photoluminescence mapping, and electrochemical impedance spectroscopy (EIS).

Results and discussion

MAPbI$_3$ perovskite films prepared from solution are usually full of surface defects,[24,25] but due to the mobile nature of these defects, solar cells based on MAPbI$_3$ show impressive power conversion efficiencies (PCE). In our previous works, we thoroughly studied the impact of gamma-rays on the structural, microscopic, chemical, and electronic properties of MAPbI$_3$. We did not find any impact of 10 kGy dose on the structure and morphology of the material. Moreover, solar cells based on MAPbI$_3$ showed remarkably good stability in comparison with mixed cation systems. However, later publications[22] showed that extreme doses beyond 10–100 kGy have a negative impact on MAPbI$_3$ and this led us to a proposal to determine the gamma-ray threshold for MAPbI$_3$ perovskite. Here, we exposed MAPbI$_3$ films and solar cells to gamma-ray doses: 3, 5, 10 and 21 kGy.

Since the photoluminescence (PL) of perovskite films is rarely homogeneous, we prepared PL maps scanned from the whole area of the sample (20 × 20 mm) to get more reliable data. Fig. 1 shows the PL mapping images of the same sample, at each point of exposure, and single-point PL spectra, averaged from PL mapping data.

As we can see, the maximum PL is at ≈ 775 nm and it does not change with dose, meaning a lack of phase transformation upon gamma-ray exposure. At 3 kGy, the PL intensity of the sample increases on all surface from an average of 25 000 to an average of 33 000 counts. This means that a 3 kGy dose improves the film quality and heals the initial energy defects in MAPbI$_3$. Further accumulation of dose on this sample results in reduction of PL intensity to the level close to the initial state. 21 kGy dose creates new traps in the material and this process dominates over initial defect healing, which leads to PL shrinking down to 8000 counts. Thus, in the range of 3–21 kGy the PL intensity of MAPbI$_3$ went through the maximum at 3 kGy and went way below the initial state at 21 kGy.

In parallel with PL mapping, we performed TRPL measurements to observe the change in recombination dynamics. It is
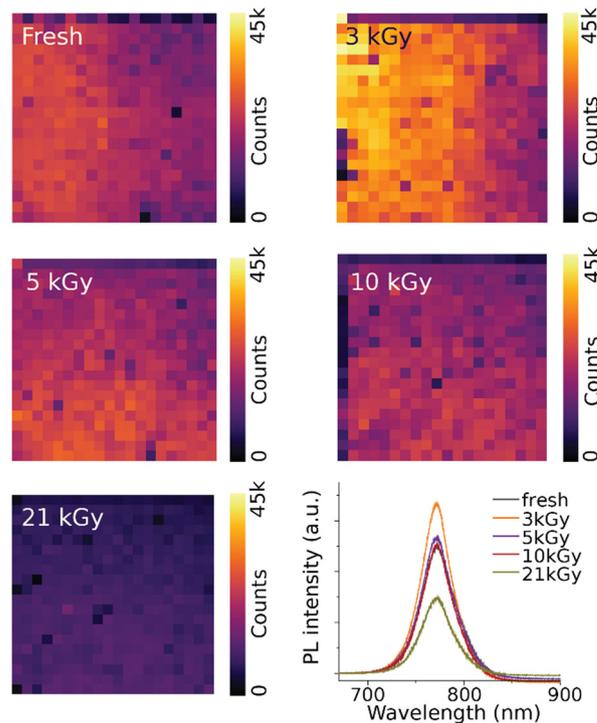

Fig. 1 PL maps of fresh and exposed (3, 5, 10, and 21 kGy) MAPbI$_3$ films and their average PL spectra.

important to highlight that these measurements were performed strictly within 2 h after gamma-ray exposure to avoid any impact of relaxation.

Fig. 2 shows the comparison of freshly prepared and exposed MAPbI$_3$ TRPL curves. The shape of the PL decay curve depends on recombination rates. If the carriers only suffer radiative recombination, the dependency of PL intensity on the time satisfies the single exponential equation:[26]

$$N(t) = Ae^{-\left(\frac{(x - x_0)}{\tau}\right)} + c,\qquad (1)$$

where A is the PL decay amplitude, x and x_0 are the times of the decay, ns, τ is the carrier lifetime, ns, and c is a constant
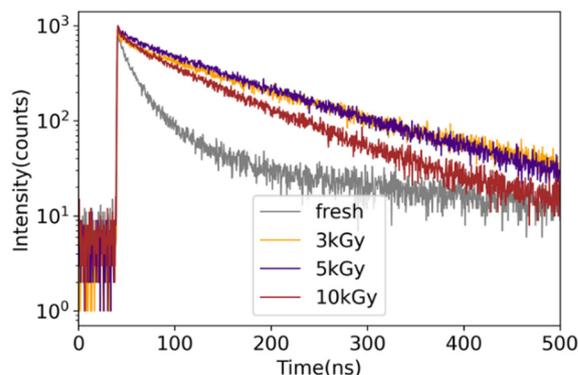

Fig. 2 TRPL curves of fresh and exposed (3, 5, and 10 kGy) samples.

characterizing diffuse light scattering background and electron noise background.

When the decay curve no longer satisfies the single exponential relationship, it is necessary to use double or triple exponential fitting. For the double exponential relation the equation is the following:

$$N(t) = A_1 e^{-\left(\frac{(x - x_0)}{\tau_1}\right)} + A_2 e^{-\left(\frac{(x - x_0)}{\tau_2}\right)} + c \qquad (2)$$

In this case, the carriers suffer both radiative and non-radiative recombination. Slow component τ_2 is responsible for slow radiative recombination, while fast component τ_1 is responsible for non-radiative trap assisted recombination, which is faster than radiative recombination.[26–28]

The average lifetime $\tau_{average}$ is further calculated as[26]

$$\tau_{average} = \sum_{i=1}^{n} A_i \tau_i^2 \bigg/ \sum_{i=1}^{n} A_i \tau_i \qquad (3)$$

Table 1 shows carrier lifetime values calculated from TRPL curves for fresh and exposed MAPbI$_3$ films.

The average carrier lifetime of the fresh sample τ_2 = 78 ns drastically increases after the 3 kGy radiation up to 135 ns and reaches a maximum of 142 ns at 5 kGy dose, reflecting the decrease of bulk defect density after irradiation, which is in accordance with PL maps. The subsequent irradiation with 10 kGy dose leads to the drop of charge carrier lifetime, which may indicate the initial photoactive layer degradation.

An additional parameter that can tell about the recombination regime is the ideality factor. For that, we prepared a set of solar cells and exposed them to the gamma source, measuring Suns-V_{OC} curves after 5, 10 and 21 kGy dose. Solar cell characteristics and external quantum efficiencies (EQE) can be found in ESI,† Fig. S1–S3, and Table 1. It can be seen that power conversion efficiencies (PCE) as well as short circuit current densities (J_{SC}) of exposed samples decrease even after 3–5 kGy doses. The main factor that contributes to PCE and J_{SC} reduction is the gamma ray induced substrate darkening. Glass transmittance decreases particularly in the 300–600 nm region.[29] Ionization generates free charge carriers that become trapped in vacancies or impurities. This creates color centers, which significantly reduce the optical transmission of glass. In our previous work[5] we conclude that substrate darkening is the predominant process affecting the MAPbI$_3$ solar cell performance, while the solar cell itself is surprisingly stable under doses up to 10 kGy (1000 krad).

Here, we went beyond 10 kGy and observed a noticeable decay in fill factor (FF), which points to growing interface recombination.

Ideality factor n_{id} does not consider interface recombination, but it can tell what is going on in the bulk of the absorber material. We performed the analysis and derived n_{id} from the Suns-V_{OC} curve for fresh and exposed solar cells using the Shockley diode equation:

$$n_{id} = \frac{q}{k_b T} \times \frac{dV_{OC}}{d\ln(I_0)} \qquad (4)$$

where q is the absolute value of electron charge, 1.6×10^{-19} Coulombs, k_b is the Boltzmann constant, 1.38×10^{-23} J K^{-1}, T is the temperature, 298 K, V_{OC} is the open circuit voltage, mV, and I_0 is the light intensity, mW cm^{-2}.

In classic theory, the boundary conditions are the following:[30,31]

n_{id} = 2 – Shockley–Read–Hall (SRH) recombination regime

n_{id} = 1 – bimolecular e–h recombination regime

However, in perovskite solar cells, redistribution of photo-generated charges, defect distributions, and recombination at the contacts complicate the interpretation.[32] It can easily go below 1 and above 2, and the SRH recombination regime can exist between 1 and 2.

Fig. 3 shows the Suns-V_{OC} dependency with n_{id} derived from the slope. Each point on the graph comes from the statistical data obtained from at least 3 different samples with 8 individual cells on each.

5 kGy dose results in an increase of V_{OC} values and a noticeable decrease in ideality factor from the initial 1.89 to 1.69. 10 kGy dose brings n_{id} back to 1.89, and V_{OC} values are lower than for 5 kGy dose. Accumulation of the 21 kGy dose results in further reduction of V_{OC}, which might point to enhanced interface recombination. The n_{id} of the 21 kGy-exposed sample is the lowest, also pointing to a strong shift towards the trap-assisted recombination regime. Thus, moderate doses reduce the concentration of traps and this

Table 1 Calculated parameters from TRPL curves

Dose	A_1	τ_1	A_2	τ_2	c	$\tau_{average}$
Fresh	95	12	137	91	10	**78**
3 kGy	503	22	88	138	5	**135**
5 kGy	158	26	20	145	6	**142**
10 kGy	476	15	56	102	6	**99**
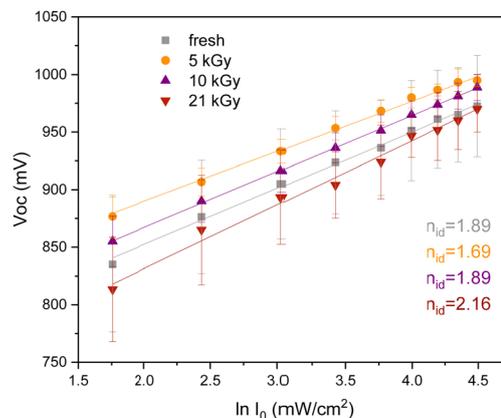
Fig. 3 Suns-V_{OC} dependency of fresh and exposed (5, 10, and 21 kGy) solar cells.

12374 | *Phys. Chem. Chem. Phys.*, 2024, **26**, 12372–12378

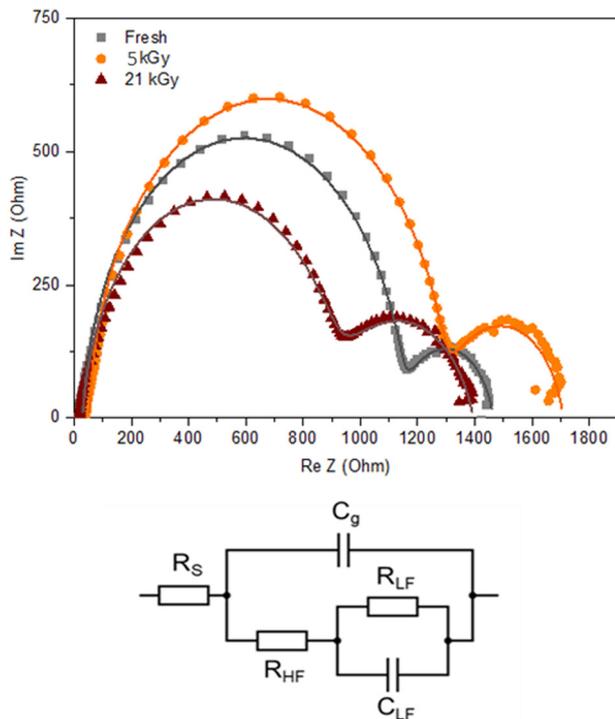This journal is © the Owner Societies 2024

Fig. 4 Nyquist plot of impedance spectra of fresh and irradiated solar cells and equivalent circuit used to fit the data.

leads to a minor shift towards the bimolecular recombination regime. Further dose accumulation eliminates the shift and n_{id} moves back to the initial 1.6. These results perfectly correlate with the PL data, discussed earlier.

Samples after 5 kGy exposure were stored in a glovebox and remeasured after 30 days. As can be observed in Fig. S4, the ESI† current density of the stored sample is slightly higher than that after exposure, which is expected, as color defect formation on glass substrates has a reversible origin. Interestingly, V_{OC} after storage reduced and became even lower than that of the fresh sample, which might point to some postponed negative effect of gamma-rays on solar cell performance. However, the PCE of the stored sample (forward scan) became even better than that of the fresh sample, again pointing to the trap healing process that occurs at low doses (3–5 kGy).

Next, we performed electrochemical impedance spectroscopy (EIS) measurements on the fresh and exposed solar cells at open-circuit voltage under illumination. Fig. 4 shows the Nyquist plots of the EIS spectra and equivalent circuit used to fit experimental curves. To account for non-ideal effects in the PSCs impedance response constant-phase elements (CPEs) were used to represent C_g and C_{LF}. The elements of this circuit are attributed to the following processes. R_s is the series resistance arising from the resistance of solar cell contacts and wires used in the measurement process. The high-frequency arc corresponds to electronic and mixed electronic-ionic processes. C_g is the geometrical capacitance arising from the dielectric properties of a perovskite layer sandwiched between two electrodes, and it depends on perovskite thickness

and properties. The corresponding resistance R_{HF} is typically regarded as recombination resistance. The low-frequency circuit corresponds to ionic conductivity and electrochemical reactions (second semicircle).[33] In general, C_{LF} is considered corresponding to charge accumulation at the interfaces. The interpretation of R_{LF}, however, is ambiguous. In some works, it is attributed to ionic conductivity.[34] However, more commonly it is viewed as another component of recombination resistance since it demonstrates similar light- and bias-dependence to R_{HF}.[35] In this work, we follow this assumption and calculate recombination resistance as $R_{rec} = R_{HF} + R_{LF}$.

Recombination describes the electron capture process, transition of charges from the conduction band to the trap states and/or valence band. Thus, the higher the resistance to this process, the better is the solar cell performance.[36]

As can be seen in Fig. 4 the HF semicircle is growing with 5 kGy dose and decreasing at 21 kGy in comparison with the fresh sample. At the same time the LF semicircle grows consistently with the increasing dose.

Table 2 shows the calculated values of each element from the equivalent circuit for the fresh and exposed samples. First of all, geometric capacitance stays almost the same for all samples, which is to be expected.

Overall, R_{rec} shows the highest value at 5 kGy with a slight decrease afterwards. It can be interpreted as the decrease of non-radiative recombination at small doses and increase at high doses. However, the counter-trends for R_{HF} and R_{LF} at high doses suggest a complex process. Given the simultaneous decrease of C_{LF} which can be interpreted as lower charge accumulation at the interfaces, one might assume that interfacial trap density constantly decreases after irradiation. However, R_{HF} decrease might point to a higher rate of bulk recombination after the irradiation.

In this way, EIS data also supports the statement about the reduction of non-radiative recombination at low doses (5 kGy) and degradation at higher doses (21 kGy).

To start the discussion on the possible mechanism observed in our experiment, one should consider the defective nature of polycrystalline perovskite films. There are many types of intrinsic and extrinsic lattice defects forming during solution deposition. Negatively charged iodine interstitials I_I, cation vacancies (V_{MA} and V_{Pb}) and the substitution MA cation (I_{MA}) and Pb (I_{Pb}) typically induce hole traps (electron donors), while halide vacancies V_I and MA cation substitutions for halide (MA_I) usually induce electron traps (electron acceptors).[24] One of the most common ways of interaction between the material and gamma photon is photoelectric effect. When the gamma photon reaches the material, it initiates the formation of an electron–hole pair and the energy transferred to the electron is

Table 2 Equivalent circuit parameters for the fresh and exposed samples

	R_s, Ohm	R_{HF}, Ohm	R_{LF}, Ohm	R_{rec}, Ohm	C_g, F	C_{LF}, F
Fresh	17	1130	306	1436	3.1E−8	3.5E−5
5 kGy	40	1250	404	1654	3.0E−8	2.5E−5
21 kGy	20	900	464	1365	3.6E−8	1.4E−5

sufficient to escape the material. Among all types of ionization sources, gamma photons create the highest fraction of unrecombined holes.[11] As MAPbI$_3$ polycrystalline films have a large number of negatively charged defects, which are typically considered as hole trap states, gamma-rays annihilate these traps with the release of secondary electrons. In particular, iodine interstitials and substitutions are especially important since they form deep-level traps.[24,25] Such deep traps contribute to nonradiative recombination, and their large concentrations significantly reduce carrier diffusion length and quality of the charge extraction. As we observed a decline in nonradiative recombination at moderate doses 3–5 kGy, the decrease of donor defect concertation is large enough to overcome the negative impact of gamma-rays on the MAPbI$_3$ film. Further accumulation of dose brings us to a saturated state, where the number of deep donor traps in the bulk becomes neglectable and formation of unrecombined holes starts to dominate, producing more acceptor defects. However, at the interfaces defect density is significantly higher than in the bulk. Hence, the dose required to eliminate them is much higher, which results in a constant decrease of interfacial charge accumulation even at high doses. Therefore, the increase of dose up to 21 kGy significantly accelerates the rate of bulk recombination and deteriorates overall performance in solar cells despite some decrease in interfacial defect density. We believe that at such doses interface recombination contributes the most to solar cell degradation.

Materials and methods

Thin film preparation

Glass substrates were cut into 2.5 cm^2 pieces, manually cleaned with acetone, and subjected to additional plasma cleaning for 300 s. 222.5 mg of methylammonium iodide (MAI) and 645.4 mg of PbI$_2$ were dissolved in 1 mL of organic solvent (DMF : NMP - 80 : 20) and stirred for 24 hours at room temperature for complete dissolution of all the components. 50 μL of the solution was deposited (dynamically) at 4000 rpm followed by quenching with 100 μL of toluene (dropped 12 s after the perovskite precursor) applied at the same spin-coating frequency. The deposited MAPbI$_3$ films were annealed for 10 min at 85 °C, which led to the development of a dark brown colour.

Solar cell fabrication

ITO substrates (15 Ohm per sq Kintec) were cleaned by sonication in deionized water, acetone, and isopropyl alcohol (IPA) for 10 min each, dried in the air and subjected to plasma cleaning (50 W, 300 s). A 10% suspension of SnO$_2$ nanoparticles (Alfa Aesar) was deposited at 4000 rpm, followed by annealing in air at 170 °C for 20 min. Next, samples were introduced into a nitrogen glovebox for deposition of all remaining layers. [6,6]-Phenyl-C61-butyric acid methyl ester (PCBA) was used as an effective passivator following the procedure described in other work.[37] The perovskite film was applied using the same method

described earlier in the film preparation section. A solution of synthesized poly-triaryl amine (PTAA, 4 mg in chlorobenzene (CHB)) was applied at 1000 rpm atop of the perovskite layer. The detailed synthesis of PTAA is described in another manuscript.[38] The samples were left to dry for 10 min inside the glove box before being loaded into the vacuum chamber for the deposition of the vanadium oxide and top electrodes. 30 nm of VO$_x$ was deposited atop the PTAA layer on the whole sample surface. Silver electrodes (100 nm) were evaporated in high vacuum (10^{-6} mbar) through a shadow mask, defining the active area of each device as ~ 0.16 cm^2.

Gamma-ray exposure

The prepared samples (thin films) were packed in Al lamination foil inside an argon glove box. Each set consisted of 8 samples, which were exposed to 3, 5, 10 and 21 kGy (2 samples per dose in the irradiation chamber with sealed ^{137}Cs gamma-ray sources ($E\gamma$ = 662 keV) with a dose rate of 2.5 Gy min^{-1} (uncertainty of dose values 10%)). Two reference samples were left fresh inside the glovebox for the same time as irradiated samples. After exposure to gamma-rays, samples were characterized with TRPL and PL within 2 hours.

IV and EQE measurements

The current–voltage characteristics of the devices were measured using an Advantest 6240A source-measurement unit under the simulated 100 mW cm^{-2} AM1.5G solar irradiation provided by the Wavelabs LS-2 AAA class solar simulator. The intensity of the illumination was adjusted using a reference silicon diode of a known spectral response. J_{SC} values were confirmed by integrating the external quantum efficiency (EQE) spectra against the standard AM1.5G spectrum. The ideality factor was calculated from V_{OC} measurements performed at different light intensity from 1 to 100%.

TRPL measurements

Time-resolved PL measurements was performed with the time correlated single photon counting (TCSPC) technique on a Horiba QuantaMaster spectrofluorometer. Peak emission was set up to 776 nm, with an entrance slit of 5 nm, time range of 1.6 μs, and 1000 counts for the peak channel.

Photoluminescence spectral measurements

Photoluminescence spectra were obtained with an Automatic Research GmbH LBIC + PL + EL microscopy setup with a Horiba spectrometer. All samples were measured at 532 nm laser wavelength with 42 μW power, at 0.05 s integration time, and 0.5 mm slit width. PL maps were taken from the 20 × 20 mm area of the samples with the following characteristics: integration time 0.05 s, slit width 0.5 mm, step size 1 mm, and integration diapason from 750 to 790 nm. PL mapping was performed in the ambient environment (RH 30%), and each sample spent ≈ 10 min in air to perform the measurements.

12376 | *Phys. Chem. Chem. Phys.*, 2024, **26**, 12372–12378

This journal is © the Owner Societies 2024

Impedance spectroscopy

The impedance spectra of perovskite solar cells were measured using an MFIA impedance analyser (Zürich Instruments) following the standard protocol.[36] To ensure accurate measurements, we have measured the cell's V_{OC} directly before the impedance measurements. The measurements were taken in the frequency range of 1 Hz–5 MHz at open-circuit voltage under illumination with 3 mW cm^{-2} white light. The AC perturbation used was 10 mV to fit the linear region of the JV curve near V_{OC}. Data fitting was performed in Python using the impedance.py package. A shadow mask was used to ensure that the same active area (0.08 cm^2) contributes to the impedance response in each case. Standard deviation of V_{OC} values lies in the 50 mV range, which is reasonably close for a meaningful comparison.[33]

Conclusions

In summary, we have explored the impact of moderate gamma-ray doses up to 21 kGy on MAPbI$_3$ thin films and solar cells. This impact was found to be nonlinear. Photoluminescence spectral response was maximum at 3 kGy, career lifetime, calculated from TRPL curves, is the largest at 5 kGy, ideality factor, found from the Suns-V_{OC} slope, is the lowest for solar cells exposed to 5 kGy and recombination resistance R_{rec} is the highest for the same 5 kGy-exposed sample. The obtained results clearly point to a gamma-ray threshold dose of 3–5 kGy, at which MAPbI$_3$ perovskite films and solar cells exhibit annihilation of initially formed trap states and reduction of parasitic nonradiative recombination. This unique property of MAPbI$_3$ makes solar cells based on the material suitable for a space environment if the total ionizing dose does not exceed 10 kGy. Moreover, a significant reduction of nonradiative recombination at 3–5 kGy dose opens up an opportunity to use gamma-ray sources as an effective method to passivate deep negatively charged traps in polycrystalline perovskite films.

Author contributions

Aleksandra Boldyreva: writing – investigation, original draft, data curation, validation; Artyom Novikov: investigation, writing – review & editing, formal analysis; Vladimir Petrov: writing – review & editing, methodology; Aleksandra Zhivchikova – investigation; Marina Tepliakova: investigation, writing – review & editing, formal analysis, visualization; Keith J. Stevenson: writing – review & editing.

Conflicts of interest

There are no conflicts to declare.

Notes and references

1 NREL efficiency chart - https://www.nrel.gov/pv/cell-efficiency.html.

2 Y. Miyazawa, M. Ikegami, T. Miyasaka, T. Ohshima, M. Imaizumi and K. Hirose, *IEEE 42nd Photovolt. Spec. Conf.*, 2015, **2015**, 1–4.

3 F. Lang, O. Shargaieva, V. V. Brus, H. C. Neitzert, J. Rappich and N. H. Nickel, *Adv. Mater.*, 2017, **1702905**, 1–22.

4 F. Lang, N. H. Nickel, J. Bundesmann, S. Seidel, A. Denker, S. Albrecht, V. V. Brus, J. Rappich, B. Rech, G. Landi and H. C. Neitzert, *Adv. Mater.*, 2016, **28**, 8726–8731.

5 A. G. Boldyreva, L. A. Frolova, I. S. Zhidkov, L. G. Gutsev, E. Z. Kurmaev, B. R. Ramachandran, V. G. Petrov, K. J. Stevenson, S. M. Aldoshin and P. A. Troshin, *J. Phys. Chem. Lett.*, 2020, **11**, 2630–2636.

6 J. R. Srour, C. J. Marshall and P. W. Marshall, *IEEE Trans. Nucl. Sci.*, 2003, **50**, 653–670.

7 G. Náfrádi, E. Horváth, M. Kollár, A. Horváth, P. Andričević, A. Sienkiewicz, L. Forró and B. Náfrádi, *Energy Convers. Manag.*, 2020, **205**, 112423.

8 Q. Xu, H. Zhang, J. Nie, W. Shao, X. Wang and B. Zhang, *Radiat. Phys. Chem.*, 2021, **181**, 109337.

9 L. Gao, K. Tao, J. Sun and Q. Yan, *Adv. Opt. Mater.*, 2022, **10**, 2102069.

10 K. Sakhatskyi, B. Turedi, G. J. Matt, E. Wu, A. Sakhatska, V. Bartosh, M. N. Lintangpradipto, R. Naphade, I. Shorubalko, O. F. Mohammed, S. Yakunin, O. M. Bakr and M. V. Kovalenko, *Nat. Photonics*, 2023, **17**, 510–517.

11 Marc Poizat, Cern - ESA - SSC Work.

12 V. V. Brus, F. Lang, J. Bundesmann, S. Seidel, A. Denker, B. Rech, G. Landi, H. C. Neitzert, J. Rappich and N. H. Nickel, *Adv. Electron. Mater.*, 2017, **3**, 1600438.

13 F. Lang, M. Jošt, J. Bundesmann, A. Denker, S. Albrecht, G. Landi, H. C. Neitzert, J. Rappich and N. H. Nickel, *Energy Environ. Sci.*, 2019, **12**, 1634–1647.

14 Y. Miyazawa, M. Ikegami, H. W. Chen, T. Ohshima, M. Imaizumi, K. Hirose and T. Miyasaka, *iScience*, 2018, **2**, 148–155.

15 K. Sakhatskyi and M. V. Kovalenko, *Light Sci. Appl.*, 2022, **11**, 41377.

16 A. García-Fernandez, B. Kammlander and S. Riva, *Phys. Chem. Chem. Phys.*, 2024, **26**, 1000–1010.

17 A. G. Boldyreva, A. F. Akbulatov, S. A. Tsarev, S. Y. Luchkin, I. S. Zhidkov, E. Z. Kurmaev, K. J. Stevenson, V. G. Petrov and P. A. Troshin, *J. Phys. Chem. Lett.*, 2019, **10**, 813–818.

18 P. Mahadik, P. Sengupta, B. Vishwanadh, S. K. Mishra, V. Sudarsan and G. K. Dey, *Radiat. Phys. Chem.*, 2017, **139**, 152–156.

19 D. Nikolić, K. Stanković, L. Timotijević, Z. Rajović and M. Vujisić, *Int. J. Photoenergy*, 2013, **2013**, 843174.

20 K. Yang, K. Huang, X. Li, S. Zheng, P. Hou, J. Wang, H. Guo, H. Song, B. Li, H. Li, B. Liu, X. Zhong and J. Yang, *Org. Electron.*, 2019, **71**, 79–84.

21 W. Bannoob, S. M. Ali and S. Aldawood, *Radiat. Phys. Chem.*, 2023, **202**, 110538.

22 V. V. Ozerova, N. A. Emelianov, D. P. Kiryukhin, P. P. Kushch, G. V. Shilov, G. A. Kichigina, S. M. Aldoshin, L. A. Frolova and P. A. Troshin, *J. Phys. Chem. Lett.*, 2023, **14**, 743–749.

This journal is © the Owner Societies 2024

Phys. Chem. Chem. Phys., 2024, **26**, 12372–12378 | **12377**

23 A. R. Kirmani, B. K. Durant, J. Grandidier, N. M. Haegel, M. D. Kelzenberg, Y. M. Lao, M. D. McGehee, L. McMillon-Brown, D. P. Ostrowski, T. J. Peshek, B. Rout, I. R. Sellers, M. Steger, D. Walker, D. M. Wilt, K. T. VanSant and J. M. Luther, *Joule*, 2022, **6**, 1015–1031.

24 H. Jin, E. Debroye, M. Keshavarz, I. G. Scheblykin, M. B. J. Roeffaers, J. Hofkens and J. A. Steele, *Mater. Horiz.*, 2020, **7**, 397–410.

25 W. Yin, T. Shi and Y. Yan, *Appl. Phys. Lett.*, 2014, **104**, 063903.

26 J. Chen, C. Zhang, X. Liu, L. Peng, J. Lin and X. Chen, *Photonics Res.*, 2021, **9**, 151.

27 E. M. Hutter, J. J. Hofman, M. L. Petrus, M. Moes, R. D. Abellón, P. Docampo and T. J. Savenije, *Adv. Energy Mater.*, 2017, **7**, 1–8.

28 B. Yang, J. Chen, S. Yang, F. Hong, L. Sun, P. Han, T. Pullerits, W. Deng and K. Han, *Angew. Chem., Int. Ed.*, 2018, **57**, 5359–5363.

29 M. F. Bartusiak and J. Becher, *Appl. Opt.*, 1979, **18**, 3342.

30 C. Van Berkel, M. J. Powell, A. R. Franklin and I. D. French, *J. Appl. Phys.*, 1993, **73**, 5264–5268.

31 T. Kirchartz, F. Deledalle, P. S. Tuladhar, J. R. Durrant and J. Nelson, *J. Phys. Chem. Lett.*, 2013, **4**, 2371–2376.

32 W. Tress, M. Yavari, K. Domanski, P. Yadav, B. Niesen, J. P. Correa Baena, A. Hagfeldt and M. Graetzel, *Energy Environ. Sci.*, 2018, **11**, 151–165.

33 E. Von Hauff and D. Klotz, *J. Mater. Chem. C*, 2022, **10**, 742–761.

34 D. Moia, I. Gelmetti, P. Calado, F. William, M. Stringer, O. Game, Y. Hu, P. Docampo, D. Lidzey, E. Palomares, J. Nelson and P. R. F. Barnes, *Energy Environ. Sci.*, 2019, **12**, 1296–1308.

35 D. Prochowicz, S. Trivedi, N. Parikh, M. Saliba, A. Kalam, M. Tavakoli and P. Yadav, *Energy Technol.*, 2021, **9**, 2100229.

36 A. Guerrero, J. Bisquert and G. Garcia-Belmonte, *Chem. Rev.*, 2021, **121**, 14430–14484.

37 S. Tsarev, T. S. Dubinina, S. Y. Luchkin, I. S. Zhidkov, E. Z. Kurmaev, K. J. Stevenson and P. A. Troshin, *J. Phys. Chem. C*, 2020, **124**, 1872–1877.

38 M. M. Tepliakova, A. V. Akkuratov, S. A. Tsarev and P. A. Troshin, *Tetrahedron Lett.*, 2020, **61**, 152317.